of the Angiosperm lineage. There are homologs with less similarity in lower plants and algae, and similarity with proteins outside of the Plantae is very low.

Applications

Although herbicide resistance has been increasing steadily since the 1970s (*23*), no new herbicide mode of action has been commercialized since the 1980s (*24*). The toxic effect of the plant-specific MDHAR6 reaction with TNT could be leveraged to develop environmentally acceptable substrates for MDHAR6 as a new class of herbicide. We therefore investigated activity of MDHAR6 toward two additional nitro-group–containing chemicals, 1-chloro-2,4-dinitrobenzene (CDNB) and 1-chloro-4-nitro-benzene (CNB), shown in Fig. 5A. Activity of purified MDHAR6, measured by following NADH oxidation, was detected toward CDNB but not CNB (Fig. 5B and fig. S8F). Measurement using HPLC demonstrated that CDNB was not depleted in assay mixtures (Fig. 5C). As observed for TNT, CDNB inhibited seedling root growth in WT Col7 seedlings on agar plates containing CDNB, with *mdhar6-1* seedlings exhibiting significantly longer roots than the wild type (Fig. 5D). These results demonstrate that MDHAR6 can reduce CDNB, with toxic effect to *Arabidopsis*, further supporting the idea that herbicidal substrates could be developed. Whereas WT seedling root lengths were reduced by ~50% in the presence of 2 μM CDNB, root lengths on 2 μM CNB were unaffected, demonstrating that CNB is significantly less phytotoxic. Alongside this result, we were unable to detect activity toward CNB using recombinant protein (Fig. 5). These results are in agreement with our hypothesis that formation of a nitro radical is the major cause of TNT toxicity in plants.

Although TNT binds to the organic and clay fractions of soil, and is thus not readily mobile in water, a common copollutant in sites contaminated with explosives is royal demolition explosive (hexahydro-1,3,5-trinitro-1,3,5-triazine) (RDX), which is highly mobile in soils and readily contaminates water supplies (*25*). Future work on effective bioremediation of explosives contamination will need both existing RDX-degrading capabilities (*26*, *27*) and resistance to the toxic copollutant TNT. Our findings explain the acute toxicity of TNT to plants and also provide an avenue by which MDHAR6 deficiency can be exploited to increase plant biomass in the presence of TNT, permitting greater rates of remediation for both TNT and RDX. Molecular breeding approaches could be used to identify deletions in *MDHAR6* orthologs, potentially enhancing TNT tolerance in relevant plant species such as switchgrass (*Panicum virgatum*), thus enabling revegetation and remediation of explosives-contaminated sites.

REFERENCES AND NOTES

1. J. Pichtel, *Appl. Environ. Soil Sci.* **2012**, 617236 (2012).
2. U.S. General Accountability Office, *Department of Defense Operational Ranges: More Reliable Cleanup Cost Estimates and a Proactive Approach to Identifying Contamination Are Needed* (GAO Publication GAO-04-601, 2004); www.gao.gov/products/GAO-04-601.
3. U.S. Agency for Toxic Substances and Disease Registry, Toxicological profile for 2,4,6-trinitrotoluene (TNT), ATSDR publication CAS 118-96-7 (ATSDR, Atlanta, 1995); www.atsdr.cdc.gov/toxprofiles/tp.asp?id=677&tid=125.
4. E. R. Travis *et al.*, *Environ. Sci. Technol.* **41**, 5854–5861 (2007).
5. E. R. Travis, N. C. Bruce, S. J. Rosser, *Environ. Pollut.* **153**, 119–126 (2008).
6. L. B. Brentner, S. T. Mukherji, S. A. Walsh, J. L. Schnoor, *Environ. Pollut.* **158**, 470–475 (2010).
7. F. Gandia-Herrero *et al.*, *Plant J.* **56**, 963–974 l(2008).
8. E. R. Beynon *et al.*, *Plant Physiol.* **151**, 253–261 (2009).
9. V. Gunning *et al.*, *Plant Physiol.* **165**, 854–865 (2014).
10. E. L. Rylott, A. Lorenz, N. C. Bruce, *Curr. Opin. Biotechnol.* **22**, 434–440 (2011).
11. D. Weigel *et al.*, *Plant Physiol.* **122**, 1003–1014 (2000).
12. O. Arrigoni, S. Dipierro, G. Borraccino, *FEBS Lett.* **125**, 242–244 (1981).
13. M. A. Hossain, K. Asada, *J. Biol. Chem.* **260**, 12920–12926 (1985).
14. C. S. Lisenbee, M. J. Lingard, R. N. Trelease, *Plant J.* **43**, 900–914 (2005).
15. K. Obara, K. Sumi, H. Fukuda, *Plant Cell Physiol.* **43**, 697–705 (2002).
16. T. Hruz *et al.*, *Adv. Bioinformatics* **2008**, 420747 (2008).
17. T. F. Jenkins *et al.*, *Chemosphere* **63**, 1280–1290 (2006).
18. C. H. Foyer, G. Noctor, *Plant Physiol.* **155**, 2–18 (2011).
19. O. W. Griffith, A. Meister, *J. Biol. Chem.* **254**, 7558–7560 (1979).
20. Y. Kumagai *et al.*, *FEBS Lett.* **478**, 295–298 (2000).
21. Y. Kumagai, M. Kikushima, Y. Nakai, N. Shimojo, M. Kunimoto, *Free Radic. Biol. Med.* **37**, 350–357 (2004).
22. S. F. Altschul, W. Gish, W. Miller, E. W. Myers, D. J. Lipman, *J. Mol. Biol.* **215**, 403–410 (1990).
23. I. Heap, The International Survey of Herbicide Resistant Weeds (1993–2015); available at www.weedscience.org.
24. S. O. Duke, *Pest Manag. Sci.* **68**, 505–512 (2012).
25. J. Clausen, J. Robb, D. Curry, N. Korte, *Environ. Pollut.* **129**, 13–21 (2004).
26. E. L. Rylott *et al.*, *Nat. Biotechnol.* **24**, 216–219 (2006).
27. R. G. Jackson, E. L. Rylott, D. Fournier, J. Hawari, N. C. Bruce, *Proc. Natl. Acad. Sci. U.S.A.* **104**, 16822–16827 (2007).
28. E. Finkelstein, G. M. Rosen, E. J. Rauckman, *Mol. Pharmacol.* **21**, 262–265 (1982).

ACKNOWLEDGMENTS

The authors acknowledge the assistance of M. V. Budarina for technical support. E.J.J., E.B., and A.L. were supported by Ph.D. studentships from the Biotechnology and Biological Sciences Research Council, the Burgess family, and the Garfield Weston Foundation, respectively. This work was supported by funding from the Strategic Environmental Research and Development Program of the U.S. Department of Defense to E.L.R and N.C.B. The supplementary materials contain additional data.

SUPPLEMENTARY MATERIALS

www.sciencemag.org/content/349/6252/1072/suppl/DC1
Materials and Methods
Figs. S1 to S8
Tables S1 and S2
References (*29*–*37*)

14 April 2015; accepted 22 July 2015
10.1126/science.aab3472

REPORTS

CHEMISTRY

Transient assembly of active materials fueled by a chemical reaction

Job Boekhoven,[1]*† Wouter E. Hendriksen,[1]† Ger J. M. Koper,[1] Rienk Eelkema,[1,2]‡ Jan H. van Esch[1,2]‡

Fuel-driven self-assembly of actin filaments and microtubules is a key component of cellular organization. Continuous energy supply maintains these transient biomolecular assemblies far from thermodynamic equilibrium, unlike typical synthetic systems that spontaneously assemble at thermodynamic equilibrium. Here, we report the transient self-assembly of synthetic molecules into active materials, driven by the consumption of a chemical fuel. In these materials, reaction rates and fuel levels, instead of equilibrium composition, determine properties such as lifetime, stiffness, and self-regeneration capability. Fibers exhibit strongly nonlinear behavior including stochastic collapse and simultaneous growth and shrinkage, reminiscent of microtubule dynamics.

Active self-assembly driven by chemical fuels is at the basis of many processes in living organisms, including cellular transport, cell motility, proliferation, and morphogenesis (*1*). Active self-assembled structures such as actin networks and microtubules (*2*) distinguish themselves from equilibrium self-assembled systems and materials (*3*) by their ability to use the free energy provided by the conversion of the fuel to achieve transient structure formation and to carry out work (*4*, *5*); in addition, their behavior is controlled by the kinetics of fuel consumption instead of by thermodynamic stability. The realization of artificial active materials created through a fuel-driven self-assembly process would further the understanding of kinetically

controlled dynamic behavior and associated spatiotemporal organization. It would also open opportunities for further developments in active separation and drug delivery, self-healing and adaptive materials, and autonomous control of chemical processes (*6*). The few artificial, chemically fueled, active self-assembling systems that have been reported typically use biological components such as DNA (*7*), enzymes (*8*, *9*), or protein building blocks (*2*, *10*, *11*), or they exploit an oscillating reaction to periodically shift the equilibrium of self-assembling (nano)particles (*12*). The need for complex biological components and oscillating reactions makes these systems expensive, complicated to use, and applicable to a limited range of working conditions. A molecular fuel-driven self-assembly process recently developed in our laboratory (*13*) showed the formation of dispersed fibrous structures with very slow dynamics, inhibiting the formation of true artificial active materials. It remains a challenge to achieve the formation of active materials where temporal material properties are controlled by fuel-conversion kinetics.

We report a general approach toward synthetic, transient, self-assembling molecular materials, driven by the consumption of chemical energy, and in which lifetime, stiffness, and regenerative behavior are controlled and can be tuned by the kinetics of fuel conversion. The system consists of simple synthetic chemicals that are commercially available on a multigram scale, and it can operate in water at room temperature, on time scales of hours to days. These active materials display nonlinear fiber dynamics, reminiscent of the dynamic instability observed in microtubules.

To arrive at a chemical fuel–driven active material, we coupled a switchable self-assembling system to a chemical reaction cycle, using the following design elements: (i) a molecule that can be switched between a nonassociating state and an associating state by the removal and reinstallment of a repulsive ionic charge; (ii) a chemical "activation" reaction between the self-assembling molecule and a sacrificial reactant (i.e., the fuel) that removes the repulsive ionic charge of the self-assembling molecule, thereby activating the self-assembling building block; (iii) a chemical "deactivation" reaction that restores the charge and returns the original charged self-assembling molecule; and (iv) different pathways for the activating and deactivating chemical reactions to form a reaction cycle, driven by the consumption of the fuel. If the activating and deactivating reactions run along the same path, adding a reactant would merely shift the chemical equilibrium, as is typically observed in triggered self-assembly processes (*14*, *15*).

Self-assembling molecules containing anionic carboxylate groups, in combination with an ester-forming carboxylate alkylation reaction (as the activating reaction) and an ester hydrolysis reaction (as the deactivating reaction), can fulfill the abovementioned requirements. The carboxylate carries a negative charge that can be removed by reaction with an alkylating electrophile fuel to form a neutral ester function. Esters can undergo spontaneous hydrolysis in aqueous environments, leading to the formation of a charged carboxylate and an alcohol waste product. As such, a carboxylate function can be used to control the molecular assembly process by changing the net charge on the molecule through kinetically controlled alkylation and hydrolysis (Fig. 1).

Kinetic analysis of the alkylation of carboxylates to drive supramolecular assembly has revealed that a substantial acceleration of the reaction kinetics (as compared with our previous study) is key to the formation of an active gel state (*13*). To reach this goal, we selected a more reactive alkylating agent and adjusted pH levels by means of a buffer to enable the formation and decay of supramolecular structures on time scales of hours, instead of 5 to 15 days (*13*). Increasing buffer concentrations resulted in a system capable of autonomously forming soft molecular materials without continuous pH adjustment and in a switch to monocarboxylates as the active gelators.

Using this system, we tested several molecular gelators (**1** to **3** in Fig. 1) containing two or three carboxylate moieties for the formation of active materials. These bis- and tris-carboxylate gelators formed isotropic aqueous solutions above the pK_a of their carboxylates (~4.5, where K_a is the acid dissociation constant). Active hydrogel materials were obtained during reaction cycles of gelators **2** or **3** with dimethyl sulfate [DMS, $(CH_3)_2SO_4$], a commercially available strong methylating agent, under hydrolytic (basic) conditions (Fig. 1). In a typical reaction cycle, the batchwise addition of DMS to buffered solutions of **1a**, **2a**, and **3a** resulted in its transient methylation, yielding methyl esters **1b**, **2b**, and **3b** (Fig. 1, A and B, and figs. S1 and S2) (*16*). Under these conditions, gelator **1** formed a

[1]Department of Chemical Engineering, Delft University of Technology, Julianalaan 136, 2628 BL Delft, Netherlands. [2]Delft Process Technology Institute, Delft University of Technology, Leeghwaterstraat 39, 2628 CB Delft, Netherlands.
*Present address: Institute for Advanced Study and Department of Chemistry, Technische Universität München, Lichtenbergstrasse 2A, 85748 Garching near Munich, Germany. †These authors contributed equally to this work. ‡**Corresponding author. E-mail: r.eelkema@tudelft.nl (R.E.); j.h.vanesch@tudelft.nl (J.H.V.E.)**

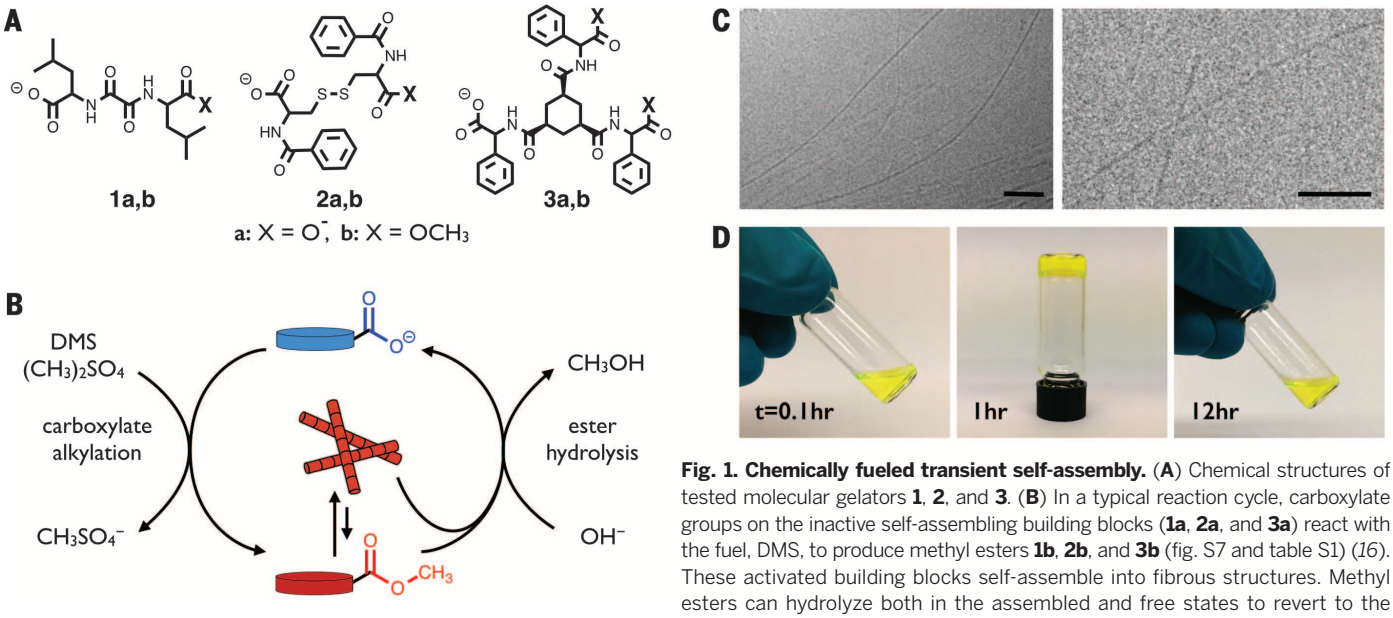

Fig. 1. Chemically fueled transient self-assembly. (**A**) Chemical structures of tested molecular gelators **1**, **2**, and **3**. (**B**) In a typical reaction cycle, carboxylate groups on the inactive self-assembling building blocks (**1a**, **2a**, and **3a**) react with the fuel, DMS, to produce methyl esters **1b**, **2b**, and **3b** (fig. S7 and table S1) (*16*). These activated building blocks self-assemble into fibrous structures. Methyl esters can hydrolyze both in the assembled and free states to revert to the original inactive building block. One full cycle produces CH_3OH (methanol) and $CH_3SO_4^-$ (MMS) as waste products. (**C**) Cryogenic transmission electron microscopy (cryo-TEM) micrographs of a gel of **2** at t = 120 min (pH 9, $[\mathbf{2a}]_0$ = 50 mM, $[DMS]_0$ = 100 mM, scale bar = 100 nm). (**D**) A typical sample in a reaction cycle (pH 11, $[\mathbf{2a}]_0$ = 50 mM, $[DMS]_0$ = 200 mM) at t = 0.1, 1, and 12 hours, with 1 μM of fluorescein added for coloring.

gelatinous precipitate but failed to form a hydrogel. We found that hydrogels of **2** and ***3*** consisted of bundles of fibers over a micrometer in length at high buffer concentrations, with individual fiber diameters of 8 and 10 nm, respectively (Figs. 1C and 4B and fig. S2) (*16*).

Focusing on gelator **2**, more detailed kinetic investigations showed that **2b** reached a critical gelation concentration typically 20 min after the addition of fuel, at which the formation of fibers resulted in macroscopic semitransparent gel materials (Fig. 1D). The critical gelation concentration of **2b** was estimated from inverted tube tests and rheology experiments to be between 0.1 and 2.8 mM, but it could not be determined accurately because of the dynamic nature of the material (tables S4 and S5) (*16*). Over time, **2b** hydrolyzed back to **2a** (Fig. 1), leading to the breakdown of the fibers and the dissolution of the gels. In a reaction cycle at the relatively low pH value of 9, the hydrolysis reaction took place at a slow rate, producing gels that persisted for weeks. Running a reaction cycle at higher pH values increased the rate of hydrolysis; as a result, the concentration of **2b** reached a maximum value, after which it decreased to zero on a time scale of hours. For instance, a gel formed at pH 11 had a lifetime of around 10 hours (*17*). Likewise, reducing the amount of fuel added at pH 11 resulted in a change in gel lifetime from 10 hours (initial fuel concentration, $[DMS]_0$ = 200 mM) to less than 4 ($[DMS]_0$ = 175 mM).

The time scales of gel formation and dissolution thus depend strongly on the reaction conditions employed. Moreover, the material properties and their time dependence change with changing reaction conditions. Hence, the reaction cycle started by gelator **2a** and DMS constitutes a fuel-driven self-assembling system that can operate autonomously, at reaction-cycle

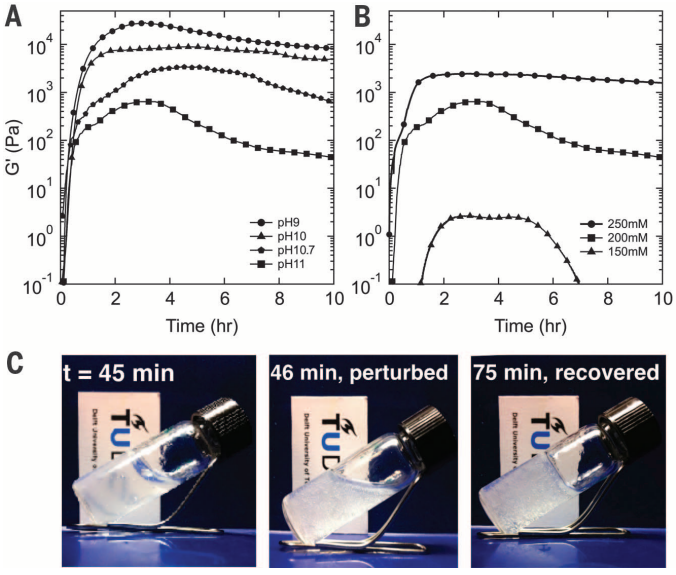

Fig. 2. Macroscopic mechanical behavior of the active material. (**A**) Rheology time sweeps of solutions of **2** during a reaction cycle at varying pH ($[DMS]_0$ = 200 mM, pH 9 to 11) and (**B**) at varying DMS concentrations ($[DMS]_0$ = 150 to 250 mM, pH 11). (**C**) Fuel-driven gel regeneration: photographs of an active gel of **2** before, immediately after, and 30 min after mechanical perturbation of the gel. In all experiments, $[\mathbf{2a}]_0$ = 50 mM.

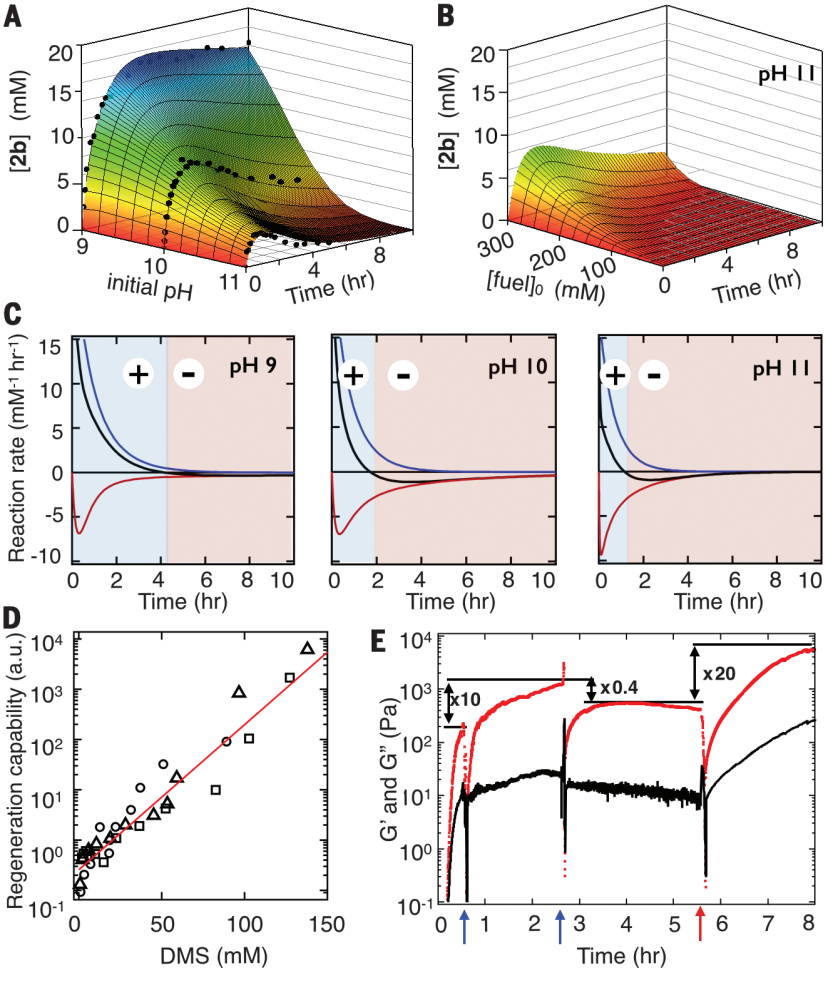

Fig. 3. Kinetics of transient gelator formation and gel regeneration. (**A** and **B**) The influence of reaction conditions on the concentration of **2b** over time. The black markers depict data points obtained from HPLC. The surface plots depict the kinetic model obtained at (A) different initial pH, with a constant initial DMS concentration, and (B) an initial pH of 11, with different initial DMS concentrations. (**C**) Rates of alkylation of **2a** (blue lines), hydrolysis of **2b** (red lines), and net formation of **2b** (black lines) against time at pH 9, 10, and 11 ($[\mathbf{2a}]_0$ = 50 mM, $[DMS]_0$ = 200 mM). Blue areas indicate net alkylation (+); red areas indicate net hydrolysis (−). (**D**) The relative regeneration of the gels, as determined by rheology, versus the concentration of remaining fuel at the moment of perturbation (square, pH 9; triangle, pH 10; circle, pH 11; $[\mathbf{2a}]_0$ = 50 mM, $[DMS]_0$ = 200 mM) (figs. S12 to S15) (*16*). (**E**) The mechanical response of a gel after perturbation and addition of new fuel (*G*', red; *G*'', black). Blue arrows at 0.5 and 2.7 hours indicate perturbation by applying strain; the red arrow at 5.5 hours indicates a perturbation and addition of 200 mM of DMS. Values between horizontal black lines indicate relative regeneration ratios.

time scales of 4 to 10 hours, and that provides access to the active gel state.

The rheology of **2**- and **3**-based active materials showed the formation of gels and a rapid increase in gel stiffness after the addition of fuel (Fig. 2A and figs. S3 to S5) (*16*). At pH 9, the near absence of a deactivating hydrolysis reaction resulted in stiff gels with persistent storage moduli (G') in the 10-kPa range and a loss factor (tan δ) of ~0.03 for **2**; for **3**, it resulted in a G' of 0.4 kPa with a tan δ of ~0.5. G' and G'' (the loss modulus) were constant over a wide frequency range, which is typical behavior for soft fibrillar gels formed from supramolecular gelators (*18*). Higher pH values resulted in less stiff gels, and, over time, a declining storage modulus was observed, with a decay rate that increased with pH. Changing the initial concentration of the fuel changed both the lifetime and the maximum stiffness of the gels, with results ranging, for instance, from short-lived, very weak gels at $[DMS]_0$ = 150 mM to much stronger gels with lifetimes of multiple days at $[DMS]_0$ = 250 mM (Fig. 2B). The observed strong dependence on fuel concentrations and pH was confirmed by a kinetic reaction model for **2**.

These materials also showed fuel-driven self-regenerating behavior after destructive mechanical perturbation. When destroyed during the first hours after the addition of fuel, gels of **2** quickly regained and surpassed the stiffness obtained before destruction (Figs. 2C, 3D, and 3E and figs. S12 to S15) (*16*). This behavior is generally not observed in conventional low–molecular weight gels near thermodynamic equilibrium. If perturbed late in the reaction cycle when the fuel was depleted, the regeneration capability dropped below one and eventually was lost completely. Thus, the mechanical and regenerative behavior of these active materials is strongly dependent on the progression of the reaction cycle. We also showed that the system can operate under continuous-flow conditions with a continuous supply of fuel, prolonging the lifetime of the material (fig. S22) (*16*).

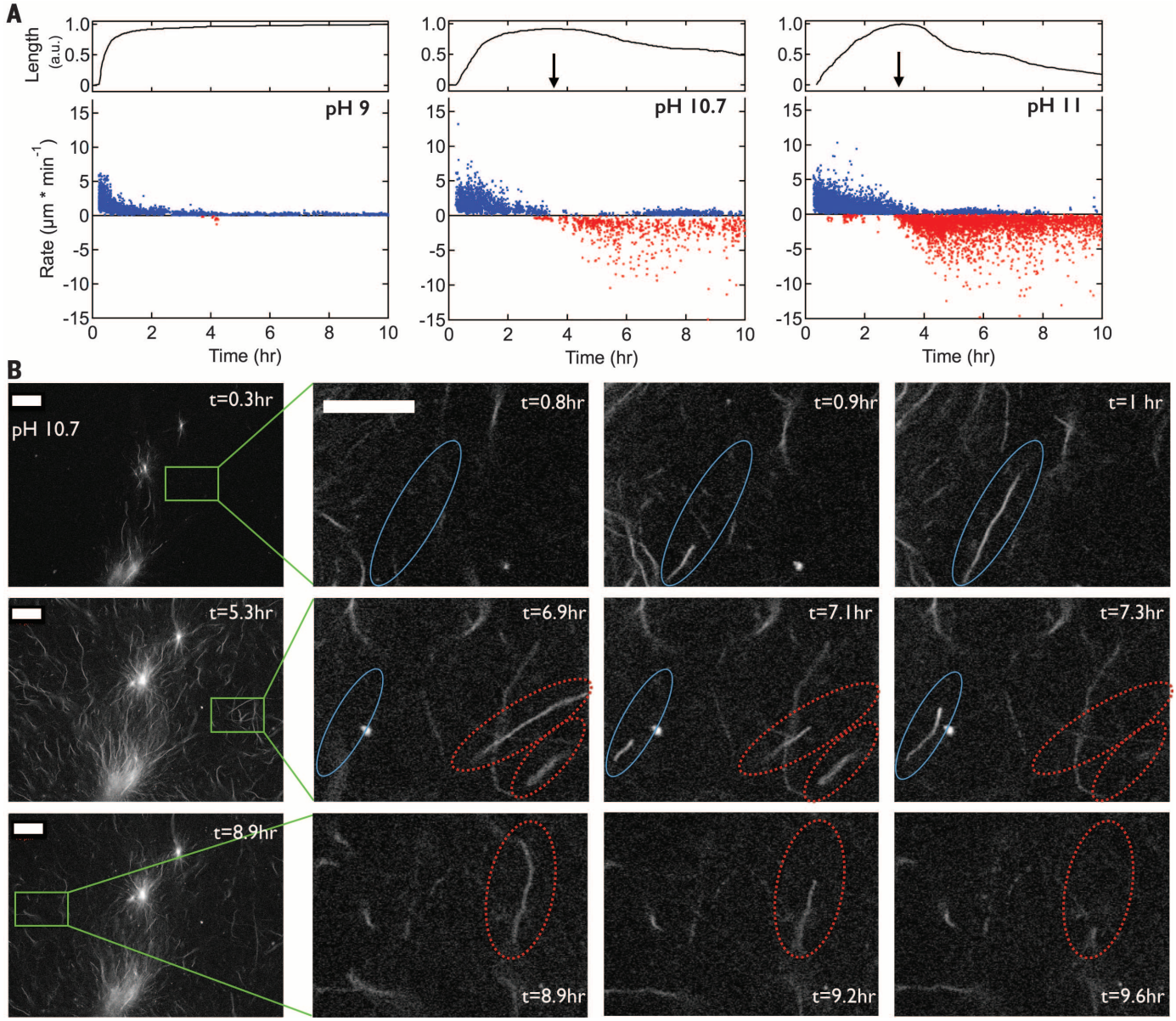

Fig. 4. Microscopic analysis of fiber dynamics. (**A**) Upper panel: normalized total fiber length against time in the reaction cycle. Arrows indicate the reaction-cycle time where G' reaches its maximum value (Fig. 2A). Lower panel: rates of fiber growth (blue) and fiber shrinkage (red), at various pH's. (**B**) Confocal micrographs over time, showing distinct fiber growth, shrinkage, and overlapping periods during a reaction cycle. Growing fibers are indicated in blue circles, and shrinking fibers are indicated in red circles. All samples were prepared with $[\mathbf{2a}]_0$ = 50 mM, $[DMS]_0$ = 200 mM, and pH 10.7. The scale bar is 10 μm.

To link the observed macroscopic behavior to the molecular-scale reactions, we performed a kinetic analysis of the active materials from gelator **2**. Starting from the pronounced dependence of gel lifetimes on fuel concentration and pH, we developed a simple kinetic model based on two competing chemical reactions: the forward alkylation of **2a** to **2b** by DMS and the reverse hydrolysis of **2b** to **2a** (Fig. 1B). The direct hydrolysis of DMS to monomethyl sulfate (MMS) was also taken into account as a separate background reaction. Using kinetic data from high-performance liquid chromatography (HPLC) and proton nuclear magnetic resonance (^{1}H-NMR) spectroscopy measurements, we determined the rate constants of all relevant reactions, allowing the construction of a kinetic model for the formation of **2b** (Fig. 3 and figs. S6 to S11) (*16*). We found that the rate of alkylation, k_1[**2a**][DMS], with k_1 = 2.5 M^{-1} $hour^{-1}$ at pH 10, followed a linear decay until all DMS had been depleted and showed a marginal variation with the pH. By contrast, the rate of hydrolysis, k_2[**2b**][OH^-], with $k_2 = 5.6 \times 10^4$ M^{-1} $hour^{-1}$ at pH 10 (table S3) (*16*), was exponentially dependent on pH. Subtracting the hydrolysis rate from the alkylation rate gives the net rate of formation of **2b** (Fig. 3C).

Using these rates, we defined two regimes through which the active gels progress. At first, the system is in a growth regime where the alkylation of **2a** is the dominant reaction. Subsequently, the system moves to the decay regime, in which hydrolysis is the dominant reaction. We then applied this model to analyze the relationship between the behavior of the system and the governing chemical reactions over time. The model showed that, unlike systems assembling near thermodynamic equilibrium, the behavior of these fueled systems evolves over time and is strongly dependent on the various reaction parameters, especially fuel levels and pH. The lifetimes of these active gels are globally connected to the period where [**2b**] is high, which is controlled by the initial reaction parameters (pH, $[\mathbf{2a}]_0$, $[DMS]_0$) and can be predicted with the kinetic model (Fig. 3, A and B). However, we observed a delay between the concentration of **2b** over time ($[\mathbf{2b}]_t$) (Fig. 3A) and the rheological behavior (Fig. 2A). This effect may indicate a nucleated growth mechanism of gel fiber formation and was not accounted for in the kinetic model.

We also observed that the gel state persisted for periods extending far beyond the time when reasonable concentrations of **2b** were present. For instance, the pH-11 system still contained a gel with G' > 50 Pa after 10 hours of reaction, even though [**2b**] had dropped below 0.6 mM after 5 hours. The dependence on reaction parameters and the transient character of the system indicates kinetically controlled states that do not reside at the thermodynamic minimum.

Using the model, we estimated the fuel concentration at any given time in the regeneration experiments. The regeneration capability (*19*) of these materials had an exponential dependence on the fuel concentration at the moment of perturbation (Fig. 3D), but it appeared to be independent of the pH, showing that this behavior is fuel-driven and is not significantly influenced by the hydrolysis rate (figs. S12 to S15) (*16*). When $[DMS]_t$ was less than 20 mM, the gels were no longer able to fully regenerate, indicating that the rate of formation of **2b**, needed for network repair, became too small. That the regeneration is fuel-driven implies that it can be restored at any time by the addition of new fuel. Indeed, the addition of fuel to a gel that was unable to regenerate restored its regeneration capability (Fig. 3E).

To gain more insight into the divergence between the time scales of the macroscopic behavior and the underlying chemical reaction network, we investigated the fiber dynamics of active gels from **2** with low and high hydrolysis rates (pH 9 to 11) using confocal microscopy (Fig. 4, figs. S16 to S21, and movies S1 to S4) (*16*). In all cases, after the addition of fuel, fiber growth was observed after a short lag period, coinciding with a rapid increase in gel stiffness (Figs. 4A and 2A). At pH 9, a rapid increase in the total fiber length was initially observed until the growth leveled off, and only a few shrinking fibers were observed (Fig. 4A). The active gels with higher hydrolysis rates (pH 10.7 to 11) also showed this rapid increase, but they reached a clear maximum, after which the fibers entered a shrinking regime and the total fiber length decreased. The transition between these two regimes coincided with the moment when the gels reached their maximum storage moduli. Both the moment of transition between regimes and the rate of decrease in the total fiber length depended on the pH and matched with the evolution of the storage moduli of the gels (Figs. 4A and 2A). Although fiber lengths decreased, a significant total fiber length persisted late in the reaction cycle, despite a negligible concentration of **2b**. All gels showed their highest level of structure (total fiber length, gel stiffness) midway through the reaction cycle.

At the microscopic level, several other unexpected observations were made (Fig. 4B). Instead of a gradual and simultaneous shrinking of all fibers, the assemblies tended to collapse stochastically with rates up to 15 μm/min (Fig. 4A). The fibers shrunk only at their tips and did not fracture or dissolve along their lengths. Also, for a certain period, both growing and shrinking fibers were observed in proximity to each other, randomly distributed throughout the microscope focal plane (Fig. 4B and figs. S18 to S21) (*16*). These observations are inconsistent with fiber dissolution driven by a decrease in [**2b**]. Instead, these findings point to hydrolysis of **2b** taking place both in the solution and within the fibers. The hydrolysis rate depends on the total concentration of **2b**, irrespective of the fraction bound in fibers (*20*). The observed fast stochastic collapse of fibers suggests that they become unstable above a certain critical hydrolysis level of **2b**, at which moment they rapidly dissolve, which may account for the discrepancies between molecular reaction rates and the macroscopic and microscopic behaviors. These observations show surprising similarities to the behavior of microtubule (de)polymerization, such as nonlinear fiber dynamics and dynamic instability, which are key ingredients in achieving out-of-equilibrium self-organization.

This work demonstrates the far-from-equilibrium self-assembly of molecular building blocks driven by a chemical fuel, leading to the transient formation of an active material. In these far-from-equilibrium materials, properties such as lifetime, stiffness, and self-regeneration capability are determined by reaction kinetics and fuel levels, rather than by equilibrium composition. These materials show nonlinear fiber dynamics reminiscent of microtubule behavior, and they constitute a key step in the development of synthetic self-organizing in out-of-equilibrium systems.

REFERENCES AND NOTES

1. E. Karsenti, *Nat. Rev. Mol. Cell Biol.* **9**, 255–262 (2008).
2. F. J. Nédélec, T. Surrey, A. C. Maggs, S. Leibler, *Nature* **389**, 305–308 (1997).
3. T. Aida, E. W. Meijer, S. I. Stupp, *Science* **335**, 813–817 (2012).
4. A. Desai, T. J. Mitchison, *Annu. Rev. Cell Dev. Biol.* **13**, 83–117 (1997).
5. G. M. Whitesides, B. Grzybowski, *Science* **295**, 2418–2421 (2002).
6. M. Fialkowski *et al.*, *J. Phys. Chem. B* **110**, 2482–2496 (2006).
7. D. Y. Zhang, R. F. Hariadi, H. M. T. Choi, E. Winfree, *Nat. Commun.* **4**, 1965 (2013).
8. S. Debnath, S. Roy, R. V. Ulijn, *J. Am. Chem. Soc.* **135**, 16789–16792 (2013).
9. C. G. Pappas, I. R. Sasselli, R. V. Ulijn, *Angew. Chem. Int. Ed.* **54**, 8119–8123 (2015).
10. F. C. Keber *et al.*, *Science* **345**, 1135–1139 (2014).
11. G. von Maltzahn *et al.*, *Adv. Mater.* **19**, 3579–3583 (2007).
12. I. Lagzi, B. Kowalczyk, D. Wang, B. A. Grzybowski, *Angew. Chem. Int. Ed.* **49**, 8616–8619 (2010).
13. J. Boekhoven *et al.*, *Angew. Chem. Int. Ed.* **49**, 4825–4828 (2010).
14. A. R. Hirst *et al.*, *Nat. Chem.* **2**, 1089–1094 (2010).
15. Y. Gao, J. Shi, D. Yuan, B. Xu, *Nat. Commun.* **3**, 1033 (2012).
16. Materials and methods are available as supporting materials on *Science* Online.
17. All pH values denote initial pH values. The pH decreases as the cycle proceeds as a result of the release of protons. The drift in pH is taken into account in the kinetic model.
18. R. G. Weiss, P. Terech, Eds., *Molecular Gels: Materials with Self-Assembled Fibrillar Networks* (Springer, Dordrecht, Netherlands, 2006).
19. The regeneration capability is defined as the ratio between the storage modulus (G') just before a strain sweep and the recovered maximum storage modulus, as determined by rheology (see the supplementary materials).
20. K. J. C. van Bommel, M. C. A. Stuart, B. L. Feringa, J. van Esch, *Org. Biomol. Chem.* **3**, 2917–2920 (2005).

ACKNOWLEDGMENTS

This work was supported by the Netherlands Organization for Scientific Research through a Vici grant (J.B. and J.H.v.E.) and a Complexity program grant (W.E.H., G.J.M.K., R.E., and J.H.v.E.). We thank E. Mendes for stimulating discussions, M. C. A. Stuart (University of Groningen) for carrying out initial cryo-TEM experiments, B. Norder for the initial rheology experiments, M. Bus for the atomic force microscopy measurements, and L. Palmer (Northwestern University) for proofreading the manuscript. The authors have no competing interests. Full data are in the supplementary materials.

SUPPLEMENTARY MATERIALS

www.sciencemag.org/content/349/6252/1075/suppl/DC1
Materials and Methods
Supplementary Text
Figs. S1 to S22
Tables S1 to S5
References (*21*–*25*)
Movies S1 to S4

19 May 2015; accepted 17 July 2015
10.1126/science.aac6103

Transient assembly of active materials fueled by a chemical reaction

Job Boekhoven, Wouter E. Hendriksen, Ger J. M. Koper, Rienk Eelkema and Jan H. van Esch (September 3, 2015)

Science **349** (6252), 1075-1079. [doi: 10.1126/science.aac6103]

Editor's Summary

Nonequilibrium transient self-assembly

In biology, the constant supply of energy can drive a system to be far from its equilibrium conditions and allow for useful work to be done. In contrast, in most synthetic systems, there is a drive toward lower energy states. Boekhoven *et al.* made a molecule that can switch between a nonassociating state and an associating state through the addition of a chemical fuel (see the Perspective by Van der Zwagg and Meijer). The lifetime, stiffness, and regenerative behavior of the self-assembled state could be controlled and tuned by the kinetics of fuel conversion.

Science, this issue p. 1075; see also p. 1056

Science (print ISSN 0036-8075; online ISSN 1095-9203) is published weekly, except the last week in December, by the American Association for the Advancement of Science, 1200 New York Avenue NW, Washington, DC 20005.